COBEM 2023 27TH INTERNATIONAL CONGRESS OF MECHANICAL ENGENEERING

ABCM Brazilian Society of Mechanical Sciences and Engineering
27th ABCM International Congress of Mechanical Engineering
December 04-08, 2023, Florianópolis-SC, Brazil

COBEM-2023-0499 H-Infinity control design for a full-vehicle suspension model with active anti-roll bar and electronic dampers

Matheus Rotava de Campos Soares
University of São Paulo, Polytechnic School, Av. Prof. Luciano Gualberto, 158, Cid. Universitária, São Paulo, SP
matheusrotava2@usp.br

Diego Colón
dcolon@lac.usp.br

Andrei Araujo Felix
andreifelix@usp.br

Carlos Alberto Arronte Delgado
carronte94@usp.br

Abstract. *This paper focuses on the modeling and control of a complete vehicle suspension system featuring an active anti-roll bar and semi-active electronic dampers, aimed at enhancing vehicle stability and safety. The vehicle model accounts for disturbances such as tire vertical displacements and wheel steering and includes inputs like control torque on the active anti-roll bar and flow rate inside the semi-active damper. Robust H-Infinity controllers are designed using MATLAB/Simulink Robust Control Toolbox for the center os mass, roll and pitch angles, which ensures system performance under varying conditions. Individual controllers are also designed for the semi-active dampers. Simulations are performed for the complete nonlinear model under the Fishhook maneuver. The simulations indicate improved vehicle stability, roll and pitch reduction, and ride safety. Future work will focus on implementing a hardware-in-the-loop (HIL) system for real-time interaction between the simulated plant and the controller within an ECU.*

Keywords: *Full-vehicle suspension system, H-Infinity controller, semi-active electronic damper, Vehicle stability.*

1. INTRODUCTION

In recent years, active and semi-active suspension systems have risen to prominence in the automotive industry due to their potential to enhance vehicular stability, safety, and ride comfort. Active suspension systems are known to be effective in providing safety and passengers comfort, but due to the associated high costs, it is frequently put outside the practical use (Falleiros and Colón (2016)). Semi-active suspension, on the other hand, present lower costs (if compared to active suspension) and uses the electronic controlled dampers (Santos *et al.* (2021)), which are very similar to a conventional passive damper, but the oil flux within the damper is controlled by a proportional valve or a pump. Another important safety device is the anti-roll bar, which can be passive or active. It this case, a closed-loop controller is associated, normally regulating the vehicle's roll angle (Paes (2018)). Passive bars are present in several commercial vehicles, but active bars are still restricted to high cost vehicles and the newly electrical driven models.

H-Infinity Control has been used in several applications due to its well known good results and easiness of application, specially in multivariable systems (Colón *et al.* (2013); Colón *et al.* (2014b)). Good references can be found in literature, like Skogestad and Postlethwaite (2005), and different ways to verify the robustness can be used, for example the structured singular value (SSV), as presented in Fernandes Pinheiro and Colón (2021), or even for nonlinear plants and controllers (Colón *et al.* (2014a)). Also, many commercial software packages aid in the design, validation and simulation processes, like the MATLAB's Robust Control Toolbox, and tutorials describe the intricate process of obtaining a controller, as for example Gu *et al.* (2014)

This paper delves into the intricacies of modeling a comprehensive vehicle suspension system, incorporating an active anti-roll bar, as in Paes (2018), and semi-active electronic dampers, as presented in Santos *et al.* (2021), while focusing on the design of H-infinity controllers for this system. The comprehensive vehicle model uses the control torque exerted on the active anti-roll bar, for example by a DC motor, and the flow rate within the semi-active damper for each wheel as inputs. The corresponding outputs includes the vehicle's roll angle, roll rate, pitch angle, pitch rate (captured by a gyroscopes), and the center of mass vertical position and rate. This model is articulated through a state-space equation that comprises 23 state variables. Measurable disturbances affecting the system are captured through the steering wheel angle and the wheels' angular speed, which influence lateral acceleration. It is to be noted that noises from the power-train and transmission are deemed negligible for the scope of this study.

In the quest for ensuring robust performance and stability under potential dangerous vehicular situations, H-Infinity

controllers are designed and simulation of these controllers are performed using MATLAB/Simulink. The controllers' performance are evaluated through standard tests like the fishhook. The simulation results exhibit improved vehicular stability, roll reduction, and enhanced ride comfort with the semi-active suspension system compared to traditional passive systems.

This work is within Brazil's "Rota 2030" program, which is an instrument implemented by the Federal Government through law no. 13,755 of December 10, 2018, by which tax incentives are granted to companies that invest in research, development, and technological innovation activities. One of the objectives of this program is the implementation of safety measures through assisted driving technologies. This work is part of the results obtained in the project SUSP-EST, that is funded by the Rota 2030 program (Ministério da Indústria (2017)). The rest of the paper is organized as follows: In section 2. the vehicle models are constructed. In section 3. the H-Infinity Controller is designed according to desirable performance and robustness. In section 4. simulations are done with the controller and the nonlinear model and in section 5. conclusions and future work suggestions are presented. The relevant model's equations gather in section 8.

2. VEHICLE MODELS

The modeling process begins with the writing of the mechanical equations. Classical references that aid in the automotive modeling are Rajamani (2006) and Jazar (2008). The car is considered as a set of constrained rigid bodies. Several methodologies can be used, like those with a Newtonian flavour presented in Coutinho *et al.*; Colón (2014); Colón (2018). For the present work, it is considered that only the car body is tri-dimensional, with the application of Newton and Euler equations. The wheel is modeled, for the vertical model, as performing the up and down motion. The tyres and the springs are considered linear. The damper initially are considered linear and afterwards a more detailed dynamic model, which includes the pressure dynamics, is adopted.

2.1 Vertical Model of the Complete Car with Active Anti-Roll Bar and Passive Dampers

In Fig. 1, it is presented a schematic diagram of the constrained rigid bodies that represents the relevant vehicle's dynamics for the vertical model. Springs, dampers and the anti-roll bars, as mentioned, are simplified. In fact, modeling a mechanism as intricate as a four-wheel vehicle necessitates certain simplifications, particularly if one is interested in obtaining a model useful for feedback controller design.

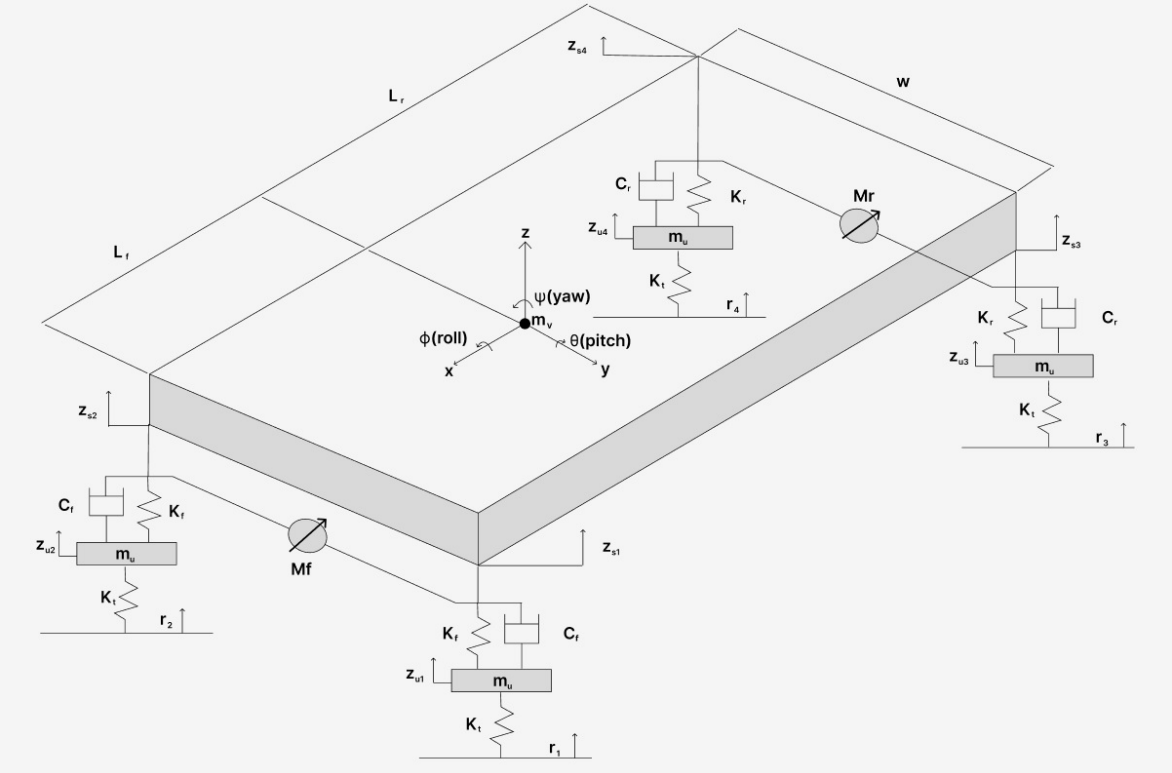

Figure 1: Complete Vertical Model with Passive Dampers

The system of linear ordinary differential equations is presented in Eq. (1) to Eq. (7). The list of model's parameters as well as the adopted values are presented in Tab. 1. This model is used the design of the H-infinity roll controllers (front and rear), as it is linear and time-invariant.

$$\mathbf{m_v}\ddot{\mathbf{z}}_\mathbf{v} = -2(\mathbf{K_f}+\mathbf{K_r})\mathbf{z_v} - 2(\mathbf{C_f}+\mathbf{C_r})\dot{\mathbf{z}}_\mathbf{v} - 2(\mathbf{L_f K_f} - \mathbf{L_r K_r})\theta - 2(\mathbf{L_f C_f} - \mathbf{L_r C_r})\dot{\theta} + \mathbf{K_f z_{u1}} + \mathbf{C_f}\dot{\mathbf{z}}_\mathbf{u1} + \mathbf{K_f z_{u2}} + \mathbf{C_f}\dot{\mathbf{z}}_\mathbf{u2} + \mathbf{K_r z_{u3}} + \mathbf{C_r}\dot{\mathbf{z}}_\mathbf{u3} + \mathbf{K_r z_{u4}} + \mathbf{C_r}\dot{\mathbf{z}}_\mathbf{u4} \quad (1)$$

$$\mathbf{I_y}\ddot{\theta} = -2(\mathbf{L_f K_f} - \mathbf{L_r K_r})\mathbf{z_v} - 2(\mathbf{L_f C_f} - \mathbf{L_r C_r})\dot{\mathbf{z}}_\mathbf{v} - 2(\mathbf{L_f^2 K_f} + \mathbf{L_r^2 K_r})\theta - 2(\mathbf{L_f^2 C_f} + \mathbf{L_r^2 C_r})\dot{\theta} + \mathbf{L_f K_f z_{u1}} + \mathbf{L_f C_f}\dot{\mathbf{z}}_\mathbf{u1} + \mathbf{L_f K_f z_{u2}} + \mathbf{L_f C_f}\dot{\mathbf{z}}_\mathbf{u2} - \mathbf{L_r K_r z_{u3}} - \mathbf{L_r C_r}\dot{\mathbf{z}}_\mathbf{u3} - \mathbf{L_r K_r z_{u4}} - \mathbf{L_r C_r}\dot{\mathbf{z}}_\mathbf{u4} \quad (2)$$

$$\mathbf{I_x}\ddot{\phi} = -\frac{\mathbf{w}^2}{2}(\mathbf{K_f}+\mathbf{K_r})\phi - \frac{\mathbf{w}^2}{2}(\mathbf{C_f}+\mathbf{C_r})\dot{\phi} + \frac{\mathbf{w}}{2}\mathbf{K_f z_{u1}} + \frac{\mathbf{w}}{2}\mathbf{C_f}\dot{\mathbf{z}}_\mathbf{u1} - \frac{\mathbf{w}}{2}\mathbf{K_f z_{u2}} - \frac{\mathbf{w}}{2}\mathbf{C_f}\dot{\mathbf{z}}_\mathbf{u2} + \frac{\mathbf{w}}{2}\mathbf{K_r z_{u3}} + \frac{\mathbf{w}}{2}\mathbf{C_r}\dot{\mathbf{z}}_\mathbf{u3} - \frac{\mathbf{w}}{2}\mathbf{K_r z_{u4}} - \frac{\mathbf{w}}{2}\mathbf{C_r}\dot{\mathbf{z}}_\mathbf{u4} \quad (3)$$

$$\mathbf{m_u}\ddot{\mathbf{z}}_\mathbf{u1} = \mathbf{K_f z_v} + \mathbf{C_f}\dot{\mathbf{z}}_\mathbf{v} + \mathbf{L_f K_f}\theta + \mathbf{L_f C_f}\dot{\theta} + \frac{\mathbf{w}}{2}\mathbf{K_f}\phi + \frac{\mathbf{w}}{2}\mathbf{C_f}\dot{\phi} - (\mathbf{K_f}+\mathbf{K_t})\mathbf{z_{u1}} - \mathbf{C_f}\dot{\mathbf{z}}_\mathbf{u1} + \mathbf{K_t r_1} + \frac{1}{\mathbf{a_{arm}}}\mathbf{M}_f \quad (4)$$

$$\mathbf{m_u}\ddot{\mathbf{z}}_\mathbf{u2} = \mathbf{K_f z_v} + \mathbf{C_f}\dot{\mathbf{z}}_\mathbf{v} + \mathbf{L_f K_f}\theta + \mathbf{L_f C_f}\dot{\theta} - \frac{\mathbf{w}}{2}\mathbf{K_f}\phi - \frac{\mathbf{w}}{2}\mathbf{C_f}\dot{\phi} - (\mathbf{K_f}+\mathbf{K_t})\mathbf{z_{u2}} - \mathbf{C_f}\dot{\mathbf{z}}_\mathbf{u2} + \mathbf{K_t r_2} - \frac{1}{\mathbf{a_{arm}}}\mathbf{M}_f \quad (5)$$

$$\mathbf{m_u}\ddot{\mathbf{z}}_\mathbf{u3} = \mathbf{K_r z_v} + \mathbf{C_r}\dot{\mathbf{z}}_\mathbf{v} - \mathbf{L_r K_r}\theta - \mathbf{L_r C_r}\dot{\theta} + \frac{\mathbf{w}}{2}\mathbf{K_r}\phi + \frac{\mathbf{w}}{2}\mathbf{C_r}\dot{\phi} - (\mathbf{K_r}+\mathbf{K_t})\mathbf{z_{u3}} - \mathbf{C_r}\dot{\mathbf{z}}_\mathbf{u3} + \mathbf{K_t r_3} + \frac{1}{\mathbf{a_{arm}}}\mathbf{M}_r \quad (6)$$

$$\mathbf{m_u}\ddot{\mathbf{z}}_\mathbf{u4} = \mathbf{K_r z_v} + \mathbf{C_r}\dot{\mathbf{z}}_\mathbf{v} - \mathbf{L_r K_r}\theta - \mathbf{L_r C_r}\dot{\theta} - \frac{\mathbf{w}}{2}\mathbf{K_r}\phi - \frac{\mathbf{w}}{2}\mathbf{C_r}\dot{\phi} - (\mathbf{K_r}+\mathbf{K_t})\mathbf{z_{u4}} - \mathbf{C_r}\dot{\mathbf{z}}_\mathbf{u4} + \mathbf{K_t r_4} - \frac{1}{\mathbf{a_{arm}}}\mathbf{M}_r \quad (7)$$

Table 1: Values of the variables used in the vehicle model.

Variable	Value	Description
m_v (kg)	1057	Mass of the center of gravity
m_u (kg)	90	unsprung mass
I_x (kg m^2)	417.4	Moment of inertia on the X-axis
I_y (kg·m^2)	2040.9	Moment of inertia on the Y-axis
I_z (kg·m^2)	2077.4	Moment of inertia on the Z-axis
L_f (m)	1.1	Distance from the front of the vehicle to the center of mass
L_r (m)	1.64	Distance from the rear of the vehicle to the center of mass
w (m)	1.43	Rear size of the vehicle
h_{cg} (m)	0.65	Height of the center of mass
r_w (m)	0.3	Size of the wheel
a_{arm} (m)	0.3	Size of the active anti-roll bar arm
K_f (N/m)	21000	Elastic constant of the front wheel springs
K_r (N/m)	23000	Elastic constant of the rear wheel springs
K_t (N/m)	190000	Tire elastic constant
C_f (Ns/m)	1000	Damping constant at the front wheels
C_r (Ns/m)	1100	Damping constant at the rear wheels
J_w (kg·m^2)	1	Inertia moment of the wheel
μ_{sx} (dimensionless)	0.8	Static friction of the tire with the ground
μ_k (dimensionless)	0.5	Friction of the moving tire with the ground
a (m^2)	0.158	Tire contact area with the ground
c_{px} (N/rad)	38000	Cornering stiffness on the X-axis
c_{py} (N/rad)	19000	Cornering stiffness on the Y-axis

In Gosselin-Brisson *et al.* (2009), an active anti-roll bar is designed for an off-road vehicle. The used model is of half-car type and the controller of the anti-roll bar is designed using linear optimal control with quadratic cost minimization. In Zulkarnain *et al.* (2012), a similar half-car model is used, but the lateral forces are modeled as the front and rear tyre

forces coming from the lateral motion of the car (yaw angle and rate variation). An active anti-roll bar controller of the PID type (proportional-integral-derivative) is designed. A more detailed model of the anti-roll bar is obtained in Paes (2018), where a more realistic geometrical form is adopted (U type anti-roll bar) which is also flexible. A Finite Element Model (FEM) is obtained for the bar and the rest of the vehicle is modeled as half-car, as the above mentioned articles. Robust H-Infinity and LQG/LTR controllers are designed and simulations for standard manouvers, like the double-lane change, are performed. Clearly the dominant modes in the bar are of torsion type.

In the present paper, the complete car model, similar to the one presented in Ibrahim *et al.* (2018), and presented in Eq. (1) to Eq. (7), is used for the design of the active anti-roll bar. The used methodology is H-infinity technique, and the details are presented in section 3.

2.2 Vertical Model of the Complete Car with Active Anti-Roll Bar and Semi-Active Dampers

An schematic representation of the complete car model with active dampers is presented in Fig. 2. The complete set of dynamic equations, including the damper pressure dynamics, is presented in the appendix (section 8).

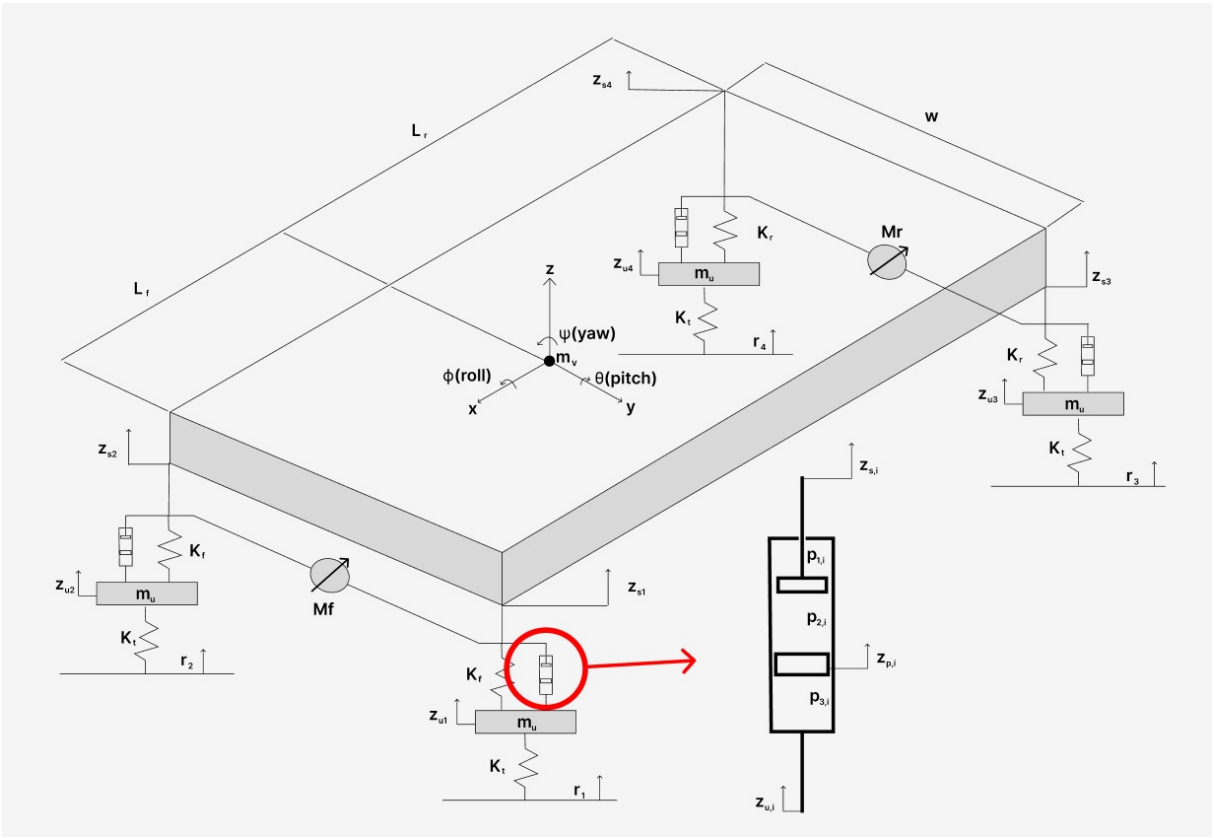

Figure 2: Complete Vertical Model with Active Dampers

This complete model, which is nonlinear, is used for simulations only and includes four sets of equations describing the dampers pressures, the equations for the degrees of freedom of the wheels (which are tied to the dampers bodies), the fluctuating pistons and pistons which are tied to the sprung mass, and the rotational and translation dynamics of the sprung mass.

2.3 Planar/Lateral Vehicle Models

In order to generate the lateral and longitudinal forces that influences the vertical model, a planar/lateral dynamic model is used. Those forces results from wheel steering imposed by the vehicles driver and are highly dependent on the tire dynamics. The Brush tire model, which is used in this work, is an anisotropic model with different cornering stiffness for lateral and longitudinal forces. Also in the model, the tire contact area is divided into two regions, one for sliding and another for adherence. The sliding region presents dynamic friction, and the adherence region has static friction. The Brush tire model uses a normalized sliding constant ($\psi_{w,i}$), where $s_{x0,i}$ and $s_{y0,i}$ are the maximum sliding possible. If $\psi_{w,i} > 1$, then only sliding occurs. If $\psi_{w,i} < 1$, then both sliding and adherence occur. In Fig. 3, a schematic representation of the Brush tire model is presented. The equations describing the planar/lateral model, including the tire model, are presented in the appendix (section 8).

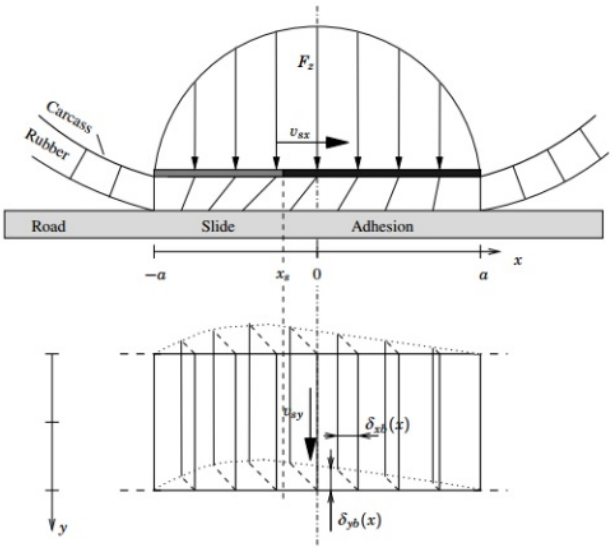

Figure 3: Brush Tire view from the side and top

3. H-INFINITY CONTROL DESIGN

The active anti-roll bar is a critical part of the vehicle suspension system, as it plays a vital role in controlling the vehicle's roll angle. On the other hand, the four dampers can also contribute to the roll stabilization, as shown in Falleiros and Colón (2016). Its design and efficiency significantly impact the vehicle's overall stability and handling, particularly during cornering and lane-changing maneuvers. The semi-active suspension system complements the anti-roll bar by mitigating the effects of vertical displacement, providing an additional degree of control over the vehicle's dynamics.

In this work, two distinct types of controllers are utilized: the first one is based on a full vehicle vertical model, and regulates the roll angle (ϕ) by means of two active anti-roll bars. The controller generates torques in the bars as outputs. The H-Infinity robust technique is the S/KS methodology, as presented in Skogestad and Postlethwaite (2005). The second controller is based on the model of a quarter car and is meant to control the semi-active dampers individually. The measured variable is the quarter car center of mass, which is replaced by the i-th piston position $z_{s,i}$. The controller output is the flow rate ($q_{1,i}$) of the i-th semi-active damper. In the full vehicle simulation, there are four controllers of this kind, one for each wheel, each of them controlling, as said above, the piston position $z_{s,i}$. For both designs, the extended plant is of the type presented in Fig. 4, where $G(j\omega)$ represents the plant to be controlled, $K(j\omega)$ represents the controller to be designed, $W_p(j\omega)$ is the performance weight function and $W_u(j\omega)$ is the control signal weight function. In order to regulate the output and reduces the influence of the disturbance d, W_p must be shaped conveniently, typically as a low pass filter. Also, high values of W_u will limit the control signal amplitudes.

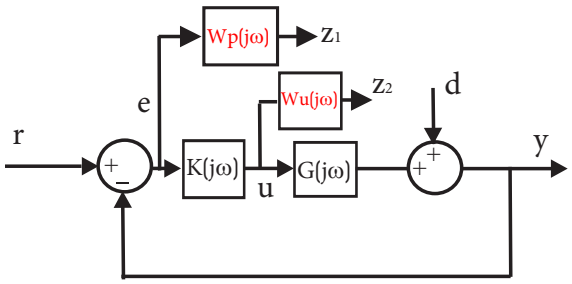

Figure 4: Extended plant for the H-infinity design.

The active anti-roll bar controller's main goal is to prevent rollovers, which mainly happen in curved trajectories, where the roll angle gradually increases. The performance weight function W_ϕ is shaped as a second order low pass Butterworth filter. The choice of a low-pass filter ensures that only the roll angle frequencies of interest are prioritized in the control effort, attenuating high-frequency noise. The cutoff frequency for this filter is set at 1 Hz, which corresponds to the significant frequency region for roll dynamics based on the vehicle parameters and driving conditions. The active anti-roll bar torques weight W_u, pondering the actuator effort, is defined as a second-order high-pass Butterworth filter.

This filter is designed to attenuate the influence of low-frequency torque actuation, thus ensuring that the controller does not demand excessive high-frequency actuator effort. For this filter, a cutoff frequency of 200 Hz is chosen. The high-pass filter was designed to allow the controller to respect the physical limitations of an expected anti-roll actuator. Both transfer functions are presented in Eq. (30).

$$\mathbf{W}_{\phi} = \frac{\mathbf{w_{0,\phi}^2}}{\mathbf{s^2} + \frac{\mathbf{2 \cdot w_{0,\phi}}}{\sqrt{\mathbf{2}}} \cdot \mathbf{s} + \mathbf{w_{0,\phi}^2}} \qquad \mathbf{W_u} = \frac{\mathbf{s^2}}{\mathbf{s^2} + \frac{\mathbf{2 \cdot w_{0,u}}}{\sqrt{\mathbf{2}}} \cdot \mathbf{s} + \mathbf{w_{0,u}^2}} \tag{8}$$

The semi-active suspension controller main goal is to minimize oscillations on the main body of the vehicle, which happen due to the natural dynamics of sprung masses. Therefore, the CM of the quarter car, which is algebraically related do the vehicle's CM, is the controlled variable. The weight performance transfer function W_z is shaped using also a second order low pass Butterworth filter, which ensures that steady-state and low frequency disturbances are penalized. The cutoff frequency for this filter is set at 10 Hz. The quarter car flow rate weight W_u, which penalizes the control effort, is defined using a second-order high-pass Butterworth filter, for the same reason as in the roll control design. For this filter, a cutoff frequency of 200 Hz is chosen. The high-pass filter was designed to allow the controller to respect the physical limitations of an expected semi-active damper, due to the low magnitude of the controller output, the weight also has a static gain of 10^4.

$$\mathbf{W_z} = \frac{\mathbf{w_{0,z}^2}}{\mathbf{s^2} + \frac{\mathbf{2 \cdot w_{0,z}}}{\sqrt{\mathbf{2}}} \cdot \mathbf{s} + \mathbf{w_{0,z}^2}} \qquad \mathbf{W_u} = \mathbf{10^4} \cdot \frac{\mathbf{s^2}}{\mathbf{s^2} + \frac{\mathbf{2 \cdot w_{0,u}}}{\sqrt{\mathbf{2}}} \cdot \mathbf{s} + \mathbf{w_{0,u}^2}} \tag{9}$$

4. SIMULATION AND VALIDATION

In order to validate the designed controllers in closed-loop, a maneuver is performed, which is the Fishhook maneuver. This is a good representation of a typical situation that occurs when the driver panics and try to recover the vehicles control. It is considered that the initial longitudinal velocity is V_x = 25 (m/s). In Fig. 5a, bottom graphic, it is shown the steering angle of the front wheels in the Fishhook maneuver. According to Forkenbrock *et al.* (2003), the maximum value for comfort is five degrees and for safety (that is, before the vehicle's rollover) is seven degrees. The roll angle is shown in the top graphic of Fig. 5a. One can see that the maximum roll angle is within the comfort and safety limits. The torque applied in the anti-roll bar is presented in the middle graphic of Fig. 5a. One clearly see that the maximum torque of the actuator (that is a DC motor) is never reached. In Fig. 5b, one can see the pitch angle, the sprung mass CM vertical position and the applied flows in the semi-active dumpers. One can see that the pitch angle stabilizes near to one degree due to the fact that the vehicle has the center of mass lightly displaced to the front. Also, the CM vertical position is around 0.65 m, as can be seen in Tab. 1. In Fig. (6a), one can see the pressures in all the twelve dampers' chambers. All the values are of typical values of conventional dampers. In Fig. 6b, the vehicle's horizontal CM position is shown. One can see that the safety is guaranteed and no rollover occurs.

5. CONCLUSIONS AND FUTURE WORK

In this paper, it was presented the design of two H-infinity controllers, one for an anti-roll bar in a model vehicle and one for a semi-active damper installed in a quarter car. Those controllers were applied to a nonlinear complete car model in order to control the roll angle and the CM position of the sprung mass. The model was submitted to a disturbance, that is, lateral forces coming from the front wheels steering in a typical Fishhook maneuver. Those forces were generated by a lateral/planar model that not is considered in the controllers design. The simulations results show that the controllers provide safety in the maneuver (that is, the car do not rollover) and the control effort is divided between the six actuators. Looking ahead, there are plans to do simulations in a hardware-in-the-loop (HIL) system, enabling real-time interaction between the plant operating in a simulation platform (such as LabCar) and the controller uploaded in an Electronic Control Unit (ECU). The development of this ECU is currently running concurrently with this project. Also, it is planed to design a multivariable controller for the complete system and compare is performance with the present system.

6. ACKNOWLEDGEMENTS

Authors would like to thank Fundação de Desenvolvimento da Pesquisa – Fundep Rota 2030 - Linha V, for the Grants SUSP-EST - *Sistema de Suspensão Semi-Ativa para Controle Avançado de Estabilidade* and SEGURAUTO - *Projeto e Desenvolvimento Integrado de Funções de Segurança Assistida ao Condutor e Ambiente para Veículos Autônomos*

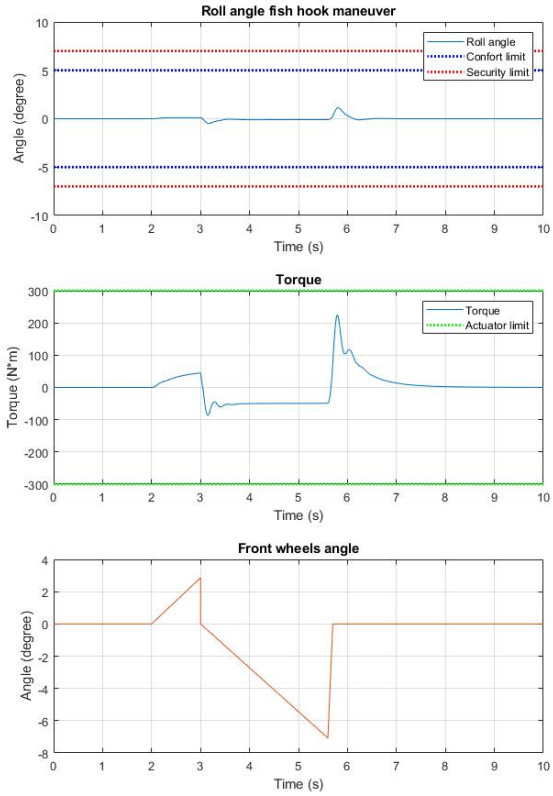

(a) Roll angle, Torque and Wheel steering.

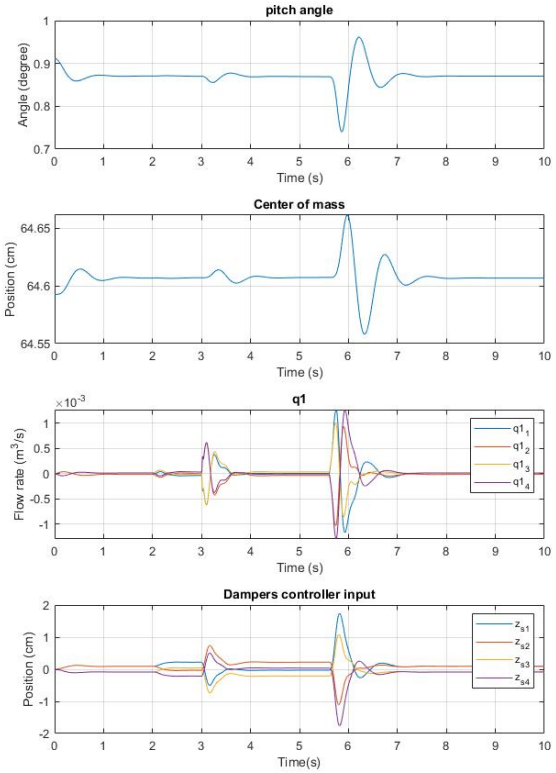

(b) Pitch angle, Center of mass position and Flow control.

Figure 5: Fishhook maneuver: main parameters

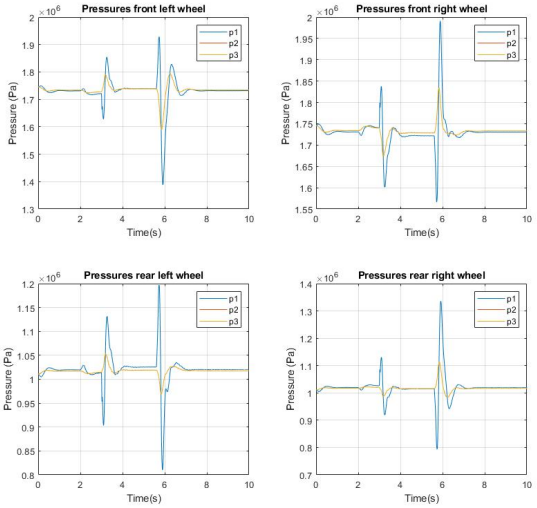

(a) Pressure in all 12 chambers

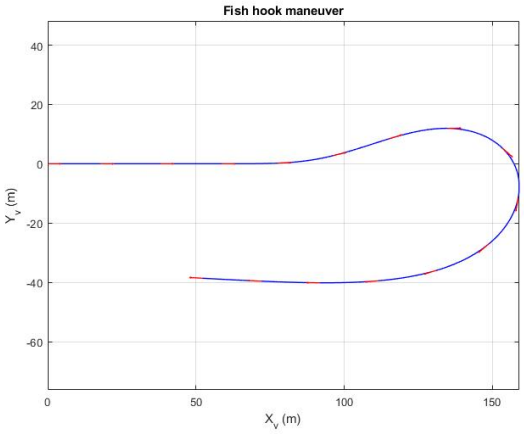

(b) Fishhook Maneuver Center of mass Position in the XY axis

Figure 6: Fishhook maneuvers: pressures and horizontal position

7. REFERENCES

Colón, D., 2014. "Connections between screw theory and cartan's connections". In *Proceedings of the Congresso Brasileiro de Automática 2014*. Sociedade Brasileira de Automatica, Belo Horizonte.

Colón, D., 2018. "Cartan connection applied to dynamic calculation in robotics". *Journal of the Brazilian Society of*

Mechanical Sciences and Engineering, Vol. 40, No. 8, p. 369. ISSN 1806-3691.

Colón, D., Balthazar, J.M., dos Reis, C.A., Bueno, A.M., Diniz, I.S. and de S. R. F. Rosa, S., 2014a. "Control design and robustness analysis of a ball and plate system by using polynomial chaos". *AIP Conference Proceedings*, Vol. 1637, pp. 226–234. doi:http://dx.doi.org/10.1063/1.4904583.

Colón, D., da Silva Ferreira, M.A., Godoy, E.P., Diniz, I.S. and Balthazar, J.M., 2013. "Identification, control design and implementation for an air heating plant". In *Proceedings of the COBEM 2013*. ABCM, Rio de Janeiro.

Colón, D., Ferreira, M.A.S., Balthazar, J.M., Bueno, A.M. and de S. R. F. Rosa, S., 2014b. "Robustness analysis of an air heating plant and control law by using polynomial chaos". *AIP Conference Proceedings*, Vol. 1637, pp. 235–244.

Coutinho, A.G., Bartholomeu, V.P., Stevani, I., de Oliveira-Fuess, J.M., Hess-Coelho, T.A. and Colón, D., ????

Falleiros, M.F. and Colón, D., 2016. "Lqg/ltr robust active suspension control applied on a nonlinear half-vehicle model". In *Proceedingd of the CBA 2016*.

Fernandes Pinheiro, R. and Colón, D., 2021. "On the μ-analysis and synthesis of mimo lurie-type systems with application in complex networks". *Circuits, Systems, and Signal Processing*, Vol. 40, No. 1, pp. 193–232. ISSN 1531-5878.

Forkenbrock, G.J., Garrott, W.R., Heitz, M. and O'Harra, B.C., 2003. "An experimental examination of double lane change maneuvers that may induce on-road, untripped, light vehicle rollover". *SAE Transactions*, Vol. 112, pp. 1128–1144.

Gosselin-Brisson, S., Bouazara, M. and Richard, M., 2009. "Design of an active anti-roll bar for off-road vehicles". *Shock and Vibration*, Vol. 16, pp. 155–174. doi:10.1155/2009/343048.

Gu, D., Petkov, P. and Konstantinov, M., 2014. *Robust Control Design with MATLAB®*. Advanced Textbooks in Control and Signal Processing. Springer London. ISBN 9781447146827.

Ibrahim, M., Abdelaziz, M., Elmarhoomy, A. and Ghoniema, M., 2018. "A 14 degrees of freedom vehicle dynamics model to predict the behavior of a golf car". *The International Conference on Applied Mechanics and Mechanical Engineering*, Vol. 18, pp. 1–21. doi:10.21608/amme.2018.34720.

Jazar, R., 2008. *Vehicle dynamics: theory and application*.

Ministério da Indústria, C.E.e.S., 2017. *Rota 2030: Propostas do Governo para uma nova política industrial automotiva. (E-book)*. Ministério da Indústria, Comércio Exterior e Serviços, Brasilia.

Paes, J.H., 2018. "A comparative study of robust control methods applied to vehicle anti-roll system by active sway bar." doi:10.11606/D.3.2019.tde-08032019-103616.

Rajamani, R., 2006. *Vehicle Dynamics and Control*.

Santos, A.O., Laganá, A.A.M. and Colón, D., 2021. "Modelagem e projeto de um amortecedor com controle eletrônico das forças de amortecimento". In *Anais do XXVIII SIMPÓSIO INTERNACIONAL DE ENGENHARIA AUTOMOTIVA*. Blucher, São Paulo, pp. 570–577.

Skogestad, S. and Postlethwaite, I., 2005. *Multivariable Feedback Control: Analysis and Design*. Multivariable Feedback Control: Analysis and Design. Wiley. ISBN 9780470011676.

Zulkarnain, N., Imaduddin, F., Zamzuri, H. and Mazlan, S.A., 2012. "Application of an active anti-roll bar system for enhancing vehicle ride and handling". pp. 260–265. doi:10.1109/CHUSER.2012.6504321.

8. APPENDIX

In this section, the complete set of dynamic equations for the model in Fig. 2 is presented. Equations (10) to (12) represent the pressure dynamics of the dampers. Equation (13) represent the oil flux between the damper chambers due to small gaps between the pistons and the damper body.

$$\dot{\mathbf{p}}_{\mathbf{1,i}} = \frac{\mathbf{E} \cdot (\mathbf{q_{1,i}} + \mathbf{q_{4,i}} + \mathbf{S_1} \cdot (\dot{\mathbf{z}}_{\mathbf{s,i}} - \dot{\mathbf{z}}_{\mathbf{u,i}}))}{\mathbf{V_1} - \mathbf{S_1} \cdot \mathbf{z}_{s,i} + \mathbf{S_1} \cdot \mathbf{z}_{u,i}} \tag{10}$$

$$\dot{\mathbf{p}}_{\mathbf{2,i}} = \frac{\mathbf{E} \cdot (-\mathbf{q_{1,i}} - \mathbf{q_{4,i}} + \mathbf{S_3} \cdot \dot{\mathbf{z}}_{\mathbf{p,i}} - \mathbf{S_2} \cdot \dot{\mathbf{z}}_{\mathbf{s,i}})}{\mathbf{V_2} - \mathbf{S_3} \cdot \mathbf{z}_{p,i} + \mathbf{S_2} \cdot \mathbf{z}_{s,i}} \tag{11}$$

$$\dot{\mathbf{p}}_{\mathbf{3,i}} = \frac{\boldsymbol{\gamma} \cdot \mathbf{p}_{3,i} \cdot (\mathbf{S_3} \cdot \dot{\mathbf{z}}_{\mathbf{u,i}} - \mathbf{S_3} \cdot \dot{\mathbf{z}}_{\mathbf{p,i}})}{\mathbf{V_3} + \mathbf{S_3} \cdot \mathbf{z}_{p,i} - \mathbf{S_3} \cdot \mathbf{z}_{u,i}} \tag{12}$$

$$\mathbf{q_{4,i}} = \boldsymbol{\pi} \cdot \mathbf{D_p} \cdot (\frac{\mathbf{b}^3 \cdot (\mathbf{p}_{2,i} - \mathbf{p}_{1,i})}{12 \cdot \mathbf{n} \cdot \mathbf{l}} - \frac{\mathbf{b} \cdot (\dot{\mathbf{z}}_{\mathbf{s,i}} - \dot{\mathbf{z}}_{\mathbf{u,i}})}{2}) \tag{13}$$

The geometrical relations presented in Eq. (14) and Eq. (15), valid for small angles, relates the sprung mass' center of mass vertical position and the piston's positions (in fact, the piston's are rigidly tied to the sprung mass). Equations (16)

relate the accelerations of the fluctuating pistons to the pressures. Equations (17) to (21) represents the vertical translation sprung mass and wheel dynamics.

$$\mathbf{z_{s,1}} = \theta \cdot \mathbf{L_f} + \phi \cdot \frac{\mathbf{w}}{2} + \mathbf{z_v} \qquad \mathbf{z_{s,2}} = \theta \cdot \mathbf{L_f} - \phi \cdot \frac{\mathbf{w}}{2} + \mathbf{z_v} \tag{14}$$

$$\mathbf{z_{s,3}} = -\theta \cdot \mathbf{L_r} + \phi \cdot \frac{\mathbf{w}}{2} + \mathbf{z_v} \qquad \mathbf{z_{s,4}} = -\theta \cdot \mathbf{L_r} - \phi \cdot \frac{\mathbf{w}}{2} + \mathbf{z_v} \tag{15}$$

$$\mathbf{\ddot{z}_{p,i}} = (\frac{\mathbf{-S_3}}{\mathbf{m_p}}) \cdot \mathbf{p}_{2,i} + (\frac{\mathbf{S_3}}{\mathbf{m_p}}) \cdot \mathbf{p}_{3,i} \tag{16}$$

$$\begin{aligned}\mathbf{m_v \ddot{z}_v} = -2(\mathbf{Kf} + \mathbf{K_r})\mathbf{z_v} - 2(\mathbf{L_f K_f} - \mathbf{L_r K_r})\mathbf{sin}(\theta) + \mathbf{K_f z_{u1}} + \mathbf{K_f z_{u2}} + \mathbf{K_r z_{u3}} + \mathbf{K_r z_{u4}} \\ -\mathbf{S_1 p_{1,1}} + \mathbf{S_2 p_{2,1}} \ - \mathbf{S_1 p_{1,2}} + \mathbf{S_2 p_{2,2}} - \mathbf{S_1 p_{1,3}} + \mathbf{S_2 p_{2,3}} - \mathbf{S_1 p_{1,4}} + \mathbf{S_2 p_{2,4}}\end{aligned} \tag{17}$$

$$\mathbf{m_u \ddot{z}_{u1}} = \mathbf{K_f z_v} + \mathbf{L_f K_f sin}(\theta) + \mathbf{K_f}\frac{\mathbf{w}}{\mathbf{2}}\mathbf{sin}(\phi) - (\mathbf{K_f} + \mathbf{K_t})\mathbf{z_{u1}} + \mathbf{S_1 p_{1,1}} - \mathbf{S_3 p_{3,1}} \ + \mathbf{K_t r_1} + \frac{\mathbf{M_f}}{\mathbf{a_{arm}}} \tag{18}$$

$$\mathbf{m_u \ddot{z}_{u2}} = \mathbf{K_f z_v} + \mathbf{L_f K_f sin}(\theta) - \mathbf{K_f}\frac{\mathbf{w}}{\mathbf{2}}\mathbf{sin}(\phi) - (\mathbf{K_f} + \mathbf{K_t})\mathbf{z_{u2}} + \mathbf{S_1 p_{1,2}} - \mathbf{S_3 p_{3,2}} \ + \mathbf{K_t r_2} - \frac{\mathbf{M_f}}{\mathbf{a_{arm}}} \tag{19}$$

$$\mathbf{m_u \ddot{z}_{u3}} = \mathbf{K_r z_v} - \mathbf{L_r K_r sin}(\theta) + \mathbf{K_r}\frac{\mathbf{w}}{\mathbf{2}}\mathbf{sin}(\phi) - (\mathbf{K_r} + \mathbf{K_t})\mathbf{z_{u3}} + \mathbf{S_1 p_{1,3}} - \mathbf{S_3 p_{3,3}} \ + \mathbf{K_t r_3} + \frac{\mathbf{M_r}}{\mathbf{a_{arm}}} \tag{20}$$

$$\mathbf{m_u \ddot{z}_{u4}} = \mathbf{K_r z_v} - \mathbf{L_r K_r sin}(\theta) - \mathbf{K_r}\frac{\mathbf{w}}{\mathbf{2}}\mathbf{sin}(\phi) - (\mathbf{K_r} + \mathbf{K_t})\mathbf{z_{u4}} + \mathbf{S_1 p_{1,4}} - \mathbf{S_3 p_{3,4}} \ + \mathbf{K_t r_4} - \frac{\mathbf{M_r}}{\mathbf{a_{arm}}} \tag{21}$$

Equation (22) represents the forces in the sprung mass. The Euler equations for the sprung mass are presented in Eq. (23) to Eq. (25) and the wheels rotational equations are of the type presented in Eq. (26). The CM translation equations are presented in Eq. (27) and Eq. (28)

$$\mathbf{F_{c,i}} = -(\mathbf{F_{spring,i}} + \mathbf{F_{damp,i}} + \mathbf{F_{arb,i}}) \qquad \mathbf{F_d} = \frac{\rho \cdot \mathbf{C_d} \cdot \mathbf{A} \cdot {\mathbf{v_{x,v}}}^2}{2} \tag{22}$$

$$\begin{aligned}(\mathbf{I_y} + \mathbf{m_v} \cdot \mathbf{z_v}) \cdot \ddot{\theta} + (\mathbf{I_x} - \mathbf{I_z}) \cdot \dot{\phi} \cdot \dot{\psi} = (\mathbf{F_{z,c3}} + \mathbf{F_{z,c4}}) \cdot \mathbf{L_r} - (\mathbf{F_{z,c1}} + \mathbf{F_{z,c2}}) \cdot \mathbf{L_f} \\ + \sum_{i=1}^{4} (\mathbf{F_{x,i}} \cdot cos(\delta_{w,i})) \cdot \mathbf{h_{cg}} + \mathbf{m_v} \cdot \mathbf{a_x} \cdot \mathbf{z_v}\end{aligned} \tag{23}$$

$$\begin{aligned}(\mathbf{I_x} + \mathbf{m_v} \cdot \mathbf{z_v}) \cdot \ddot{\phi} + (\mathbf{I_z} - \mathbf{I_y}) \cdot \dot{\theta} \cdot \dot{\psi} = (\mathbf{F_{z,c1}} - \mathbf{F_{z,c2}}) \cdot \frac{\mathbf{w}}{2} + (\mathbf{F_{z,c3}} - \mathbf{F_{z,c4}}) \cdot \frac{\mathbf{w}}{2} \\ + \sum_{i=1}^{4} (\mathbf{F_{y,i}} \cdot cos(\delta_{w,i})) \cdot \mathbf{h_{cg}} + \mathbf{m_v} \cdot \mathbf{a_y} \cdot \mathbf{z_v}\end{aligned} \tag{24}$$

$$\begin{aligned}\mathbf{I_z} \cdot \ddot{\psi} = \sum_{i=1}^{2} (\mathbf{F_{x,i}} \cdot sen(\delta_{w,i}) + \mathbf{F_{y,i}} \cdot cos(\delta_{w,i})) \cdot \mathbf{L_f} \ - \sum_{i=3}^{4} (\mathbf{F_{x,i}} \cdot sen(\delta_{w,i}) + \mathbf{F_{y,i}} \cdot cos(\delta_{w,i})) \cdot \mathbf{L_r} \\ - \sum_{i=1}^{2} (\mathbf{F_{x,i}} \cdot sen(\delta_{w,i}) + \mathbf{F_{y,i}} \cdot cos(\delta_{w,i})) \cdot \mathbf{L_r} \ - \sum_{i=3}^{4} (\mathbf{F_{x,i}} \cdot sen(\delta_{w,i}) + \mathbf{F_{y,i}} \cdot cos(\delta_{w,i})) \cdot \mathbf{L_r}\end{aligned} \tag{25}$$

$$\mathbf{I_w} \cdot \dot{\omega}_{\mathbf{w,i}} = \mathbf{T_{prop,i}} - \mathbf{T_{brake,i}} - \mathbf{F_{x,i}} \cdot \mathbf{r_w} \tag{26}$$

$$\mathbf{m_v} \cdot \mathbf{a_{x,v}} = \sum_{i=1}^{4} \mathbf{F_{x,i}} \cdot cos(\delta_{w,i}) - \sum_{i=1}^{4} \mathbf{F_{y,i}} \cdot sen(\delta_{w,i}) - \mathbf{F_d} \tag{27}$$

$$\mathbf{m_v} \cdot \mathbf{a_{y,v}} = \sum_{i=1}^{4} \mathbf{F_{y,i}} \cdot cos(\delta_{w,i}) + \sum_{i=1}^{4} \mathbf{F_{x,i}} \cdot sen(\delta_{w,i}) \tag{28}$$

The equations describing the tire planar dynamics, the Brush model, are presented in Eq. 29 to Eq. 39

$$\psi_{\mathbf{w,i}} = \sqrt{(\frac{\mathbf{s_{x,i}}}{\mathbf{s^0_{x,i}}})^2 + (\frac{\mathbf{s_{y,i}}}{\mathbf{s^0_{y,i}}})^2} \tag{29}$$

$$\mathbf{v_{xw,i}} = \mathbf{v_{x,v}} \cdot cos(\delta) + \mathbf{v_{y,v}} \cdot sin(\delta) \qquad \mathbf{v_{yw,i}} = -\mathbf{v_{x,v}} \cdot sin(\delta) + \mathbf{v_{y,v}} \cdot cos(\delta) \tag{30}$$

$$\mathbf{s_{x,i}} = -\frac{\mathbf{v_{xw,i}} - r_w \cdot \omega_{\mathbf{w,i}}}{max(abs(r_w \cdot \omega_{\mathbf{w,i}}), 0.01)} \qquad \mathbf{s_{y,i}} = -\frac{\mathbf{v_{yw,i}}}{max(abs(r_w \cdot \omega_{\mathbf{w,i}}), 0.01)} \tag{31}$$

$$\mathbf{s_{xy,i}} = \sqrt{\mathbf{s_x}^2 + \mathbf{s_y}^2} \qquad \mathbf{s^0_{x,i}} = \frac{3 \cdot \mathbf{F_z} \cdot \mu_{sx}}{2 \cdot a^2 \cdot c_{px}} \qquad \mathbf{s^0_{y,i}} = \frac{3 \cdot \mathbf{F_z} \cdot \mu_{sy}}{2 \cdot a^2 \cdot c_{py}} \tag{32}$$

if $(\psi_{\mathbf{w,i}} < 1)$ (33)

$$\mathbf{F_{tx,i}} = -c_{px} \cdot \mathbf{s_{x,i}} \cdot (1 - \psi_{\mathbf{w,i}})^2 - \mathbf{F_{z,i}} \cdot \frac{\mathbf{s_{x,i}}}{\max(\mathbf{s_{xy,i}}, 0.01)} \cdot \mu_k \cdot {\psi_{\mathbf{w,i}}}^2 \cdot (3 - 2 \cdot \psi_{\mathbf{w,i}})$$

else (34)

$$\mathbf{F_{tx,i}} = \mathbf{F_{z,i}} \cdot \frac{\mathbf{s_{x,i}}}{\max(\mathbf{s_{xy,i}}, 0.01)} \cdot \mu_k$$

if $(\psi_{\mathbf{w,i}} < 1)$ (35)

$$\mathbf{F_{ty,i}} = -c_{py} \cdot \mathbf{s_{y,i}} \cdot (1 - \psi_{\mathbf{w,i}})^2 - \mathbf{F_{z,i}} \cdot \frac{\mathbf{s_{y,i}}}{\max(\mathbf{s_{xy,i}}, 0.01)} \cdot \mu_k \cdot {\psi_{\mathbf{w,i}}}^2 \cdot (3 - 2 \cdot \psi_{\mathbf{w,i}})$$

else (36)

$$\mathbf{F_{ty,i}} = \mathbf{F_{z,i}} \cdot \frac{\mathbf{s_{y,i}}}{\max(\mathbf{s_{xy,i}}, 0.01)} \cdot \mu_k$$

$$\mathbf{F_i} = \sqrt{\mathbf{F_{tx}}^2 + \mathbf{F_{ty}}^2} \tag{37}$$

$$\mathbf{F_{x,i}} = \mathbf{F_i} \cdot \frac{\mathbf{s_{x,i}}}{max(\mathbf{s_{xy,i}}, 0.001)} \tag{38}$$

$$\mathbf{F_{y,i}} = \mathbf{F_i} \cdot \frac{\mathbf{s_{y,i}}}{max(\mathbf{s_{xy,i}}, 0.001)} \tag{39}$$

9. RESPONSABILITY NOTICE

The authors, Matheus Rotava de Campos Soares, Diego Colón, Andrei Araujo Felix e Carlos Alberto Arronte Delgado are solely responsible for the printed material included in this paper